CHEMISTRY OF MATERIALS

pubs.acs.org/cm

Article

Anti-correlation between Band gap and Carrier Lifetime in Lead Halide Perovskites under Compression Rationalized by Ab Initio Quantum Dynamics

Wei Li,* Zhi Chen, Jianfeng Tang, and Oleg V. Prezhdo*

Cite This: *Chem. Mater.* 2020, 32, 4707−4715

Read Online

ACCESS | Metrics & More | Article Recommendations | Supporting Information

ABSTRACT: Lead halide perovskites have revolutionized the solar cell community. Further optimization of perovskite-based optoelectronic devices requires fundamental understanding of their structure−property relationships. Recent experiments indicate that $MAPbI_3$ and other lead halide perovskites exhibit an unusual pressure dependence of photophysical properties. Typically, decreased band gaps are associated with shorter excited state lifetimes; however, perovskites show the opposite trend. Moreover, the narrower band gap and longer carrier lifetime achieved simultaneously form a favorable combination for solar energy utilization. We rationalize the surprising observation using ab initio nonadiabatic molecular dynamics. Compression of the inorganic lattice enhances the antibonding interaction between the Pb-s and I-p orbitals, raising the valence band maximum and decreasing the band gap. Pressure-induced destabilization of the lattice enhances fluctuations of the Pb and I atoms. The induced disorder localizes electrons and holes, decreasing their overlap. As a result, loss of coherence during the nonradiative relaxation is accelerated, and the relaxation is slowed down. This time-domain decoherence effect is equivalent to the reduction of the Franck−Condon factor in the energy domain, taking place because of a stronger response of the destabilized Pb−I lattice to photoexcitation. The detailed atomistic understanding of the structure−property relationships of lead halide perovskites paves the way for further improvement of perovskite-based optoelectronic devices.

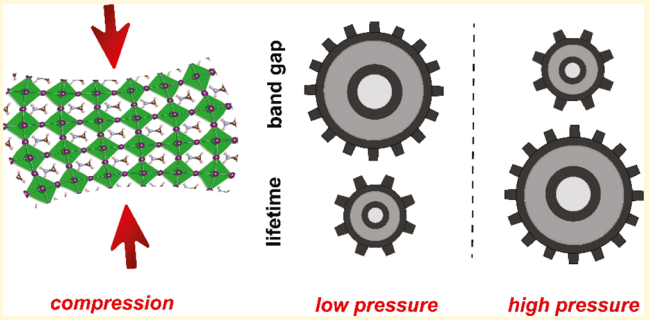

Methylammonium (MA) lead halide, $MAPbX_3$ (X = Cl, Br, I), and related perovskites have been under extensive investigations for solar cell applications owing to their high photo-to-current conversion efficiency, low cost, and ease of fabrication.[1−8] The efficiency of perovskite solar cells has increased rapidly from 3.8% in 2009 to 25.2% in 2019.[9] The prominent photovoltaic performance originates from a large optical absorption coefficient, long charge carrier diffusion, and slow carrier recombination. To approach the Shockley−Queisser efficiency limit,[10] equaling to 33.7% for a single junction semiconductor solar cell under typical sunlight conditions, the semiconductor band gap should match an optimal energy of 1.34 eV. However, the band gap of the most common $MAPbI_3$ perovskite, ∼1.6 eV, is larger than the optimal value. There exist numerous strategies to adjust perovskite band gaps.[11−13] Further optimization of perovskites toward higher luminescence efficiency requires prolongation of charge carrier lifetimes and elimination of nonradiative recombination losses. Such efforts necessitate fundamental understanding of the relationship between the perovskite structure and charge carrier dynamics at the atomistic level.

In view of the soft and dynamic nature of the inorganic lattice of metal halide perovskites, it is important to explore how perturbation to the crystal structure changes the optoelectronic performance. Pressure treatment can compress the lattice and tune the electronic structure, which can result in novel physical properties. Several teams used hydrostatic pressure to precisely regulate the compressible perovskite crystal structure.[14−21] In response to pressure, lead halide perovskites experience changes in the Pb−X bond lengths and the Pb−X−Pb bond angles, allowing one to modulate perovskite structural and electronic properties without the need to adjust the chemical compositions.

Investigation of charge carrier dynamics in perovskites is a relatively unexplored area, especially computationally, because it requires unconventional simulation tools, such as those developed in our group.[22,23] Such investigations are particularly important because carrier lifetime is one of the key parameters that determine solar cell performance. Recently,

Received: March 26, 2020
Revised: May 11, 2020
Published: May 12, 2020

https://dx.doi.org/10.1021/acs.chemmater.0c01287
Chem. Mater. 2020, 32, 4707−4715

investigations of pressure-induced effects in MA and formamidinium (FA)-based lead halide perovskites have uncovered unusual phenomena, associated with structure changes and charge recombination dynamics.[18,21,24,25] By applying mild pressure, Kong et al. have demonstrated that the $[PbI_6]^{4-}$ octahedra in $MAPbI_3$ undergo substantial distortions, resulting in simultaneous band gap narrowing and carrier lifetime prolongation.[24] Such inverse correlation between the band gap and the lifetime is unexpected because according to the common arguments, such as the energy gap law,[26] lower energy gaps are associated with reduced excited state lifetimes. Similar observations have been reported for the fully inorganic $CsPbX_3$ (X = Cl, Br, I).[27,28] The mechanism of the unusual behavior remains unclear, and a detailed atomistic investigation of charge carrier dynamics is needed in order to clarify the origin of the anti-correlation between the semiconductor band gap and charge carrier lifetime in metal halide perovskites under structural perturbations that can be induced by external pressure, strain from a substrate, and doping with larger or smaller A-site cations.

In this work, we rationalize the atomistic and quantum mechanical origins of the surprising and beneficial combination of decreased band gap and increased charge carrier lifetimes in $MAPbI_3$ under pressure. By combining time-domain density functional theory (DFT) and nonadiabatic (NA) molecular dynamics (MD), we study systematically geometric structure and MD of $MAPbI_3$, its electronic properties, elastic and inelastic electron−vibrational interactions, and the quantum dynamics of nonradiative recombination of charge carriers at three different pressures. Our simulations demonstrate that external pressure can slow down the carrier relaxation and decrease the band gap, in agreement with the experimental observations. We find that pressure-induced shortening of the Pb−I bonds enhances the antibonding coupling between the Pb-s and I-p orbitals, which form the valence band maximum (VBM), raises the VBM energy, and narrows the band gap. Increased pressures destabilize the inorganic Pb−I lattice and enhance its fluctuations, while at the same time inhibiting motions of the MA cations. The increased lattice disorder leads to localization of electron and hole charge densities and decreases their overlap. The enhanced fluctuations of the Pb and I atoms, which support electrons and holes, and the disorder-induced charge localization shorten quantum coherence time for the nonradiative charge recombination and prolong the charge carrier lifetime. Equivalently in the energy representation, the Pb−I lattice disrupted by pressure responds more strongly to photoexcitation, resulting in a larger Huang−Rhys factor and Stokes shift, and a smaller Franck−Condon factor, and hence, reduced charge recombination rate. The in-depth understanding of the band gap modulation, structural properties, and electron−vibrational relaxation in metal halide perovskites under pressure and strain obtained from the simulations assists in the design of high-efficiency perovskite-based optoelectronic devices.

To simulate the electron−hole recombination process in the $MAPbI_3$ perovskite under different pressures, Figure 1, we use the semiclassical decoherence-induced surface hopping (DISH) approach[29] for NA-MD, implemented in the framework of time-domain DFT within the PYthon eXtension for Ab Initio Dynamics (PYXAID) software package.[22,30] The lighter electrons are treated quantum mechanically, while the heavier nuclei are described classically. Decoherence effects that should arise within the electronic subsystem due to

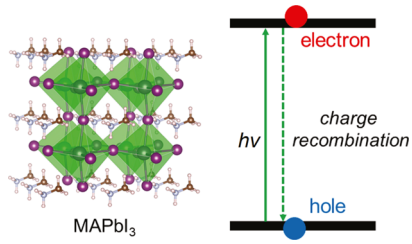

Figure 1. Illustration of cubic $MAPbI_3$ perovskite (left) and nonradiative electron−hole recombination (right).

interactions with quantum nuclei are included in DISH semiclassically, with the decoherence time estimated as the pure-dephasing time of the optical response theory.[31] The PYXAID implementation of DISH employs the classical path approximation (CPA), which uses the ground state nuclear trajectory to drive the electron dynamics. The CPA is valid in most nanoscale and condensed matter systems that undergo no photo-chemistry. It drastically reduces the computational cost and is essential for application of ab initio NA-MD to large condensed matter systems. The approach has been widely used to investigate charge carrier dynamics in many systems,[32−40] including perovskites.[41−52]

The simulations are performed on the bulk $MAPbI_3$ perovskite in the cubic phase. $MAPbI_3$ exists in both tetragonal and cubic phases and undergoes the tetragonal-to-cubic phase transition as the temperature is raised above 327 K. The simpler cubic phase allows us to perform a more systematic analysis by considering fewer non-equivalent degrees of freedom and atomic motions. Further, solar cells often operate at high temperatures in warm climates. In addition, temperature is defined in ab initio simulations up to a few tens of degrees due to a finite and relatively small size of simulation cells. We choose the cubic $MAPbI_3$ structure with the experimental lattice constants, $a = b = c = 6.3$ Å,[53] as the initial configuration. The MA cation can have different orientations, which indirectly influences the opto-physical properties of $MAPbI_3$.[54−56] We set the MA orientation in the ⟨111⟩ direction according to Giorgi et al.[57] The uncompressed lattice corresponds to ambient conditions (1 atm ≈ 0 GPa). By gradually decreasing the lattice parameter by 1 and 3%, the cubic $MAPbI_3$ structure under pressures of 1.31 and 2.73 GPa can be obtained. These pressure values are taken as the average of the stress tensor in x, y, z directions.

The electronic structure calculations, geometry optimization, and adiabatic MD are carried out using the VASP code.[58,59] The Perdew−Burke−Ernzerhof (PBE) functional is used to account for the electron exchange and correlation effects. The valence electrons are treated explicitly using the plane-wave basis set with a 500 eV energy cutoff. Both geometry optimization and adiabatic MD employ a 5 × 5 × 5 Monkhorst−Pack k-point mesh. During the geometry optimization, the atomic positions are allowed to change until the force on each atom is less than 0.01 eV/Å. The optimized structures are used to bring the temperature of all systems to 300 K using repeated velocity rescaling. The heated systems are additionally equilibrated in the *NVE* ensemble for several ps, to ensure that the temperature does not drift. Then, 4 ps *NVE* MD trajectories are obtained to perform the NA-MD calculations. The NA couplings (NACs) are computed along the equilibrated MD trajectories and are iterated three times for the DISH simulation. 2000 initial geometries are sampled

https://dx.doi.org/10.1021/acs.chemmater.0c01287
Chem. Mater. 2020, 32, 4707−4715

from the trajectories and are used as initial conditions. 1000 random number sequences are sampled for each initial condition.

Spin−orbit coupling (SOC) is significant in systems with heavy elements such as Pb and I. Previous theoretical investigations indicated that inclusion of SOC reduces the $MAPbI_3$ band gap by approximately 1 eV,[60,61] whereas bare DFT functionals without SOC produce satisfactory band gaps due to cancellation of the self-interaction error with the neglect of SOC. In principle, accurate band gaps can be obtained in both 2D and 3D perovskites by combining SOC with hybrid functionals[62] or more advanced many-body GW quasiparticle corrections.[63] However, such levels of theory are too computationally expensive for the NA-MD simulations, which involve thousands of repeated electronic structure calculations. Because the PBE functional gives a good value of the $MAPbI_3$ band gap, we employ it without SOC. Such level of theory has been used successfully to study charge carrier dynamics in lead halide perovskites.[41,48,64−68]

The calculated Pb−I bond lengths, Pb−I−Pb bond angles, and electronic energy gap in $MAPbI_3$ under 0, 1.31, and 2.73 GPa are listed in Table 1. Figure 2 presents evolution of the Pb−I bond lengths and the Pb−I−Pb bond angles, while Figure S1 presents the band structure and projected density of states (pDOS) under the compressive strain. The Pb−I−Pb bond angle decreases at elevated pressures, indicating that compression increases $[PbI_6]^{4-}$ octahedral tilting. The Pb−I bond length shortens with the application of pressure. The changes of the structural parameters influence notably the electronic properties of $MAPbI_3$. The band edge states are particularly important for the present study, as they directly participate in the electronic transition leading to charge recombination. The band structure and pDOS plots show that all systems have direct band gaps and that the band gap redshifts with increasing pressure. It is known that the VBM is a result of antibonding coupling between the Pb-s and I-p orbitals, while the conduction band minimum (CBM) is formed by nonbonding Pb-p orbitals.[69] The contraction of the Pb−I bond length and the Pb−I−Pb bond angle leads to complicated changes in the band edge states. On the one hand, the decreased Pb−I−Pb bond angle and the $[PbI_6]^{4-}$ octahedral tilting reduce the antibonding overlap of the Pb-s and I-p orbitals in the VBM, and therefore, the VBM energy should decrease, as reported by others[70,71] and in our previous works.[48,67] On the other hand, a shorter Pb−I bond increases the antibonding overlap of the Pb-s and I-p orbitals, lifting the VBM energy. The effect of the shorter Pb−I bonds outcompetes the influence of the smaller Pb−I−Pb angles, and ultimately, the antibonding orbital overlap between the Pb-s and I-p orbitals increases with applied pressure. As a result, the electronic energy gap is reduced.

Table 1. Ensemble Averaged Pb−I Bond Length (d), Pb−I−Pb Bond Angle (θ), Energy Gap (E_g), Standard Deviation of Band gap Fluctuation (σ_E), Averaged Absolute NAC, Pure-Dephasing Time (T_2^*), and Nonradiative Lifetime (T_1) for Carrier Decay in $MAPbI_3$ under Different Pressures

	d (Å)	θ (deg)	E_g (eV)	σ_E (eV)	NAC (meV)	T_2^* (fs)	T_1 (ps)
0 GPa	3.202	167.9	1.67	0.154	1.04	4.4	245.3
1.31 GPa	3.189	163.5	1.62	0.219	1.44	3.3	283.9
2.73 GPa	3.129	161.8	1.56	0.241	1.56	2.7	348.8

In addition to the energy gap, the timescale of the nonradiative charge recombination is determined by the NA electron−phonon coupling. The NAC between states i and j is given by

$$\text{NAC} = i\hbar\langle\varphi_i|\nabla_R|\varphi_j\rangle\cdot\dot{R} \quad (1)$$

Here, $\langle\varphi_i|\nabla_R|\varphi_j\rangle$ is the quantum electronic matrix element, dependent on wavefunction overlap and wavefunction sensitivity to nuclear motion. R represents nuclear coordinates, and the dot denotes the time derivative, $\dot{R} = dR/dt$. Both the electronic matrix element, $\langle\varphi_i|\nabla_R|\varphi_j\rangle$, and the nuclear velocity, $\dot{R}$, influence the NAC magnitude. We do not compute the $\langle\varphi_i|\nabla_R|\varphi_j\rangle$ matrix element separately during the NA-MD calculations because it is a highly multi-dimensional vector. Instead, we obtain the $i\hbar\langle\varphi_i|\nabla_R|\varphi_j\rangle\cdot\dot{R}$ product directly, which is a scalar.

In order to characterize the overlap-type $\langle\varphi_i|\nabla_R|\varphi_j\rangle$ matrix element, we compute the overlap of the VBM and CBM charge densities for 100 structures sampled from the MD trajectories, Figure 3. The photo-generated charge carriers relax rapidly to

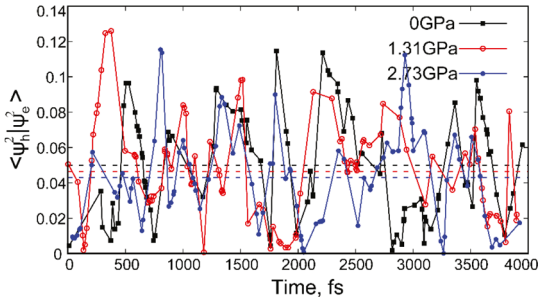

Figure 3. Overlap of VBM and CBM charge densities for 100 structures sampled from the MD trajectory. Increased pressure drives fluctuation of the $[PbI_6]^{4-}$ inorganic lattice and localizes and separates electrons and holes.

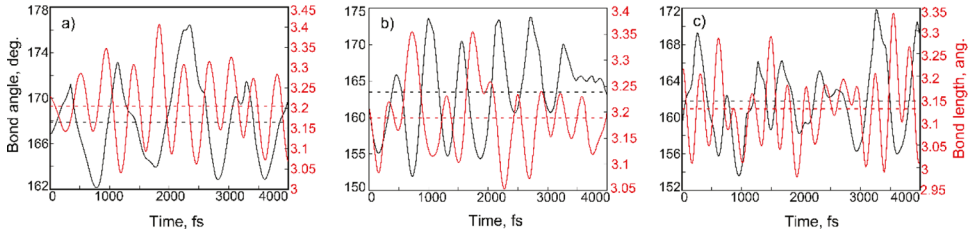

Figure 2. Evolution of the Pb−I bond length (red) and the Pb−I−Pb bond angle (black) at the pressures of (a) 0 GPa, (b) 1.31 GPa, and (c) 2.73 GPa. The dashed lines denote the ensemble average values.

https://dx.doi.org/10.1021/acs.chemmater.0c01287
Chem. Mater. 2020, 32, 4707−4715

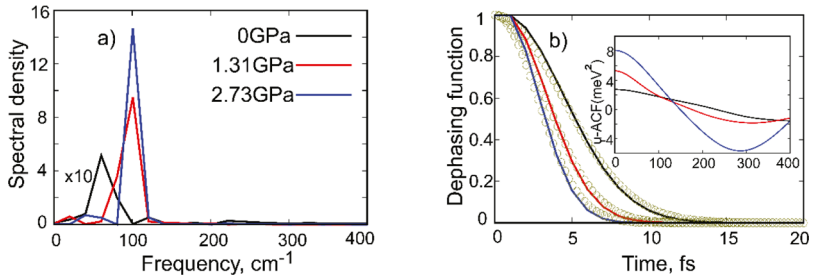

Figure 4. (a) Spectral densities and (b) pure-dephasing functions for $MAPbI_3$ at 0 GPa (black line), 1.31 GPa (red line), and 2.73 GPa (blue line). The inset in part (b) shows un-normalized ACFs of the energy gap fluctuations. The signals are stronger at higher pressure because Pb and I atomic motions are enhanced, Table S1.

the band-edge states, and therefore, the VBM−CBM charge density overlap characterizes the extent of electron−hole interactions during the recombination process. Even though the charges are localized next to each other within the simulation cell, their overlap is quite small, less than 10%. This is because electrons and holes are supported by different atomic orbitals, and because thermal fluctuations of atoms create instantaneous disorder that tends to localize the charges in different spatial parts of the simulation cell. The overlap fluctuates significantly during the MD trajectory, ranging from essentially 0 to over 10%. A fluctuation between 0 and 10% takes a few hundred femtoseconds, required to tilt the $[PbI_6]^{4-}$ octahedra. The ensemble averaged values of the electron−hole overlap decrease with pressure: 5.0, 4.6, and 4.3% at 0, 1.31, and 2.73 GPa, respectively. This trend already rationalizes why the charge carrier lifetime increases with pressure. Compression perturbs the ideal structure of the inorganic lattice, creating disorder that enhances charge localization. The enhanced disorder is also evidenced by the larger band gap fluctuations at higher pressures, Table 1. Note that larger energy gap fluctuations typically correspond to faster loss of quantum coherence for the corresponding electronic transition[72] and faster decoherence extends the transition time, as manifested by the quantum Zeno effect.[73]

Because the NAC is proportional to the atomic velocity, eq 1, we compute the ensemble averaged velocities of the Pb, I, and MA atoms, Table S1. The Pb and I atoms exhibit stronger fluctuations at higher pressures, which is consistent with the decreased electron−hole overlap, Figure 3, and increased band gap fluctuation, Table 1. Interestingly, the MA cations fluctuate less at higher pressures. This is because compression of the inorganic Pb−I lattice shrinks the $[PbI_6]^{4-}$ octahedra and leaves less space for motion of the MA cations. This agrees with previous reports that higher pressure locks the reorientations of MA cations in $MAPbI_3$.[74−76] The motions of the Pb−I and MA subsystems present yet another unusual anti-correlation between metal halide perovskites properties, in addition to the band gap-lifetime anti-correlation. The enhanced velocities of the Pb and I atoms at higher pressures lead to larger NACs, Table 1, even though the electron−hole overlap decreases slightly, Figure 3.

In addition to the band gap and NAC, the nonradiative electron−hole recombination time is influenced by the quantum coherence time, which is a time-domain equivalent of the Franck−Condon factor[77] and is closely related to the Huang−Rhys factor and Stokes shift. Faster decoherence corresponds to a larger Huang−Rhys coupling parameter, a smaller integrated Franck−Condon factor, and a slower transition. We evaluate the quantum coherence time as the pure-dephasing time of the optical response theory,[31] employing the second-order cumulant expansion that accelerates convergence. The pure-dephasing time can be measured directly using photon-echo experiments or obtained as the inverse of the homogeneous linewidth available from single-chromophore luminescence measurements. First, we compute the unnormalized autocorrelation function (ACF) of the VBM−CBM energy gap

$$C(t) = \langle \Delta E(t) \Delta E(0) \rangle_T \tag{2}$$

where $\Delta E(t) = E(t) - \langle E \rangle$ is deviation of the instantaneous energy gap from its ensemble averaged value. The square root of the initial ACF value, $C(0) = \langle E^2(0) \rangle_T$, gives the magnitude of the energy gap fluctuation listed in Table 1. The decoherence function is obtained by double integration of the ACF

$$D(t) = \exp\left[-\frac{1}{\hbar^2} \int_0^t \mathrm{d}t' \int_0^{t'} \mathrm{d}t'' C(t'') \right] \tag{3}$$

The decoherence functions and ACFs are shown in Figure 4. The decoherence/pure-dephasing times are obtained by fitting $D(t)$ to Gaussians, $\exp(-t^2/2\tau^2)$, and their values are listed in Table 1.

The Franck−Condon factor can be obtained from the decoherence function as its Fourier transform (FT) evaluated at the quantum transition frequency.[77] However, converging such calculation is very difficult in the condensed phase and nanoscale systems for transitions across energy gaps on the order of 1 eV. This is because FT of the Gaussian-shaped pure-dephasing function arising from the second-order cumulant approximation, eqs 2 and 3, gives a Gaussian-shaped dependence of the Franck−Condon factor on the transition energy. Evaluation at energies on the order of 1 eV gives 0, indicating that a much more accurate evaluation of the tail of the pure-dephasing function is required. Such a task is extremely difficult to achieve computationally at the ab initio level of description because it requires very long MD trajectories. In contrast, incorporation of decoherence into a quantum dynamics calculation gives reliable results, which can be tested both against experimental lifetimes and linewidths.[78]

Quantum coherence is an important topic of investigation in a broad spectrum of applications, ranging from charge and energy transport in biological and nanoscale systems for light-harvesting[72,79] to quantum information processing.[80] In the majority of such studies, long coherence times are required. In contrast, long charge carrier lifetimes are achieved with short coherence because short coherence slows down the quantum transitions responsible for charge trapping and recombina-

https://dx.doi.org/10.1021/acs.chemmater.0c01287
Chem. Mater. 2020, 32, 4707−4715

tion.[73,81] Indeed, the decoherence/pure-dephasing times for all systems are short, only a few femtoseconds: 4.4, 3.3, and 2.7 fs for 0, 1.31, and 2.73 GPa, respectively, Table 1. Because the pure-dephasing functions are obtained from the ACF, eqs 2 and 3, the inset of Figure 4b, ACF analysis provides additional insights. Pure-dephasing is fast, if the initial value of the unnormalized ACF, representing the energy gap fluctuation, is large.[72] By destabilizing the structure, compression enhances the energy gap fluctuations, rationalizing the faster decoherence.

In order to characterize the phonon modes that participate in the charge-phonon scattering, we obtained spectral densities by computing FTs of the energy gap ACFs

$$I(\omega) = \left| \frac{1}{\sqrt{2}} \int_{-\infty}^{+\infty} \mathrm{d}t \; \mathrm{e}^{-\mathrm{i}\omega t} C(t) \right|^2 \tag{4}$$

The spectral densities show signals at 100 cm^{-1} and below, Figure 4a. The frequencies are low because the band edge states are supported by the heavy Pb and I elements. According to the experimental Raman characterization of $MAPbI_3$ single crystals, such phonon frequencies can be assigned to the Pb−I bending and stretching motions,[82] which are well represented already by the perovskite unit cell. Participation of only the low frequency vibrations leads to a generally weak NA electron−phonon coupling and slow nonradiative charge recombination, Table 1. The intensity of the signals in Figure 4a is directly related to the amplitude of the phonon-induced energy gap fluctuations. The larger the FT amplitude, the larger the gap fluctuation, and the faster the pure-dephasing.

Finally, we perform NA-MD simulations in order to characterize theoretically the pressure dependence of the charge carrier lifetimes in cubic $MAPbI_3$. Figure 5 shows

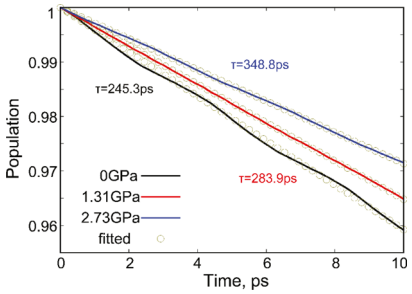

Figure 5. Excited-state population decay in $MAPbI_3$ at different pressures. Nonradiative electron−hole recombination is slower at higher pressures because of faster pure-dephasing/decoherence, in agreement with the experiment.

evolution of the population of the lowest energy excited state corresponding to the band gap excitation. Charges generated by photo-excitations at energies above the band gap rapidly relax to the band gap via intraband relaxation,[83,84] and therefore, the studied process represents nonradiative charge carrier recombination for sunlight of any frequency above the band gap. The initial short-time component of the carrier relaxation obtained in the NA-MD simulations can be approximated by the first-order expansion of the exponential decay, $f(\tau) = \exp(-t/\tau) \approx 1 - t/\tau$. The nonradiative relaxation times, τ, are presented in Table 1. The electron−hole recombination time for $MAPbI_3$ under ambient conditions (the 0 GPa system) is 245 ps, which is about an order of magnitude faster than the experimentally reported nanosecond electron−hole recombination time.[1] The difference can be attributed to the small size of simulation cell, limited by the computational efforts. Charges form large polarons[85] and small simulation cells tend to overestimate the electron−phonon coupling. Further, the NA-MD simulations assume that charges have already approached each other and are localized within the simulation cell. In experiments, charges take time to diffuse around the sample before interacting, get trapped and de-trapped, scatter off surfaces and grain boundaries, and so on. The charge recombination time increases with pressure, agreeing with the experimental observation.[24] Slower charge recombination leads to better solar cell performance, because it allows for longer-lived charge carriers, and minimizes charge and energy losses. By applying external pressure, one can influence the perovskite geometric and electronic structure, and its dynamical response, in order to achieve simultaneous redshift of the energy gap and prolongation of the charge carrier lifetimes, both of which are very beneficial for sunlight harvesting and solar energy utilization.

The pressure dependence of the nonradiative electron−hole recombination time can be explained by the interplay of the electronic energy gap, the NA electron−phonon coupling, and the pure-dephasing/decoherence time, which are listed in Table 1. Generally, an electronic transition is slow if the NA electron−phonon coupling is weak, the electronic energy gap is large, and quantum coherence is short-lived. In turn, the NAC depends on an overlap type matrix element involving the electron and hole wavefunctions and atomic velocity, eq 1. The NAC grows with pressure, Table 1, even though the overlap of the electron and the hole decreases, Figure 3. The NAC increases because velocities of the Pb and I atoms grow, Table S1. The energy gap decreases with pressure, Table 1. Therefore, both the NAC and the energy gap favor faster relaxation with increasing pressure, contrary to the experiment[24] and our calculations. Thus, decoherence/pure-dephasing is the only factor that rationalizes the longer charge carrier lifetime at higher pressures. The decoherence time is the time-domain analog of the Franck−Condon factor defined in the energy domain,[77] and both are closely related to the Huang−Rhys factor and Stokes shift. Faster decoherence corresponds to a smaller Franck−Condon factor. Increased pressures destabilize the inorganic Pb−I lattice and make it more responsive to changes in the electronic structure. Photo-excitation perturbs the lattice more strongly at higher pressures, decreases the Franck−Condon factor, and shortens quantum coherence. As a result, the nonradiative transition slows down, and the charge carriers live longer. Interestingly, this phenomenon is a direct manifestation of the quantum Zeno effect.[73]

The current simulations followed the standard protocol for periodic systems, employing the $MAPbI_3$ unit cell, periodic boundary conditions, and multiple k-points. The charges are delocalized over multiple simulation cell images implicitly present in such calculation setup. Only one k-point is used for the charge recombination simulation because $MAPbI_3$ is a direct band gap semiconductor. The simulation cell size creates limitations on representation of atomic motions. The number of vibrational motions contributing to the NAC and decoherence is limited by the number of atoms in the simulation cell. Thus, in principle, the NAC and decoherence rate can be underestimated. However, both NAC and decoherence arise from stretching and bending motions already present in the unit cell. The same phonons have

https://dx.doi.org/10.1021/acs.chemmater.0c01287
Chem. Mater. 2020, 32, 4707−4715

been identified in calculations with larger simulation cells.[86] The size of the simulation cell also limits the range of pressure-induced deformations to the system geometry, and hence, the extent of disorder-induced localization of electrons and holes. Larger simulation cells would allow more electron−hole separation. However, if the crystal structure is maintained under pressure, the charges will remain delocalized over large parts of the material (much larger than any practical simulation cell size), and the changes in the electron−hole overlap, Figure 3, are already captured with the current simulation cell.

The original experiment by Kong et al.[24] indicated that the $MAPbI_3$ perovskite undergoes a phase transition with increasing pressure from *I*4/*mcm* to *Imm*2. The band gap narrows at mild pressures and increases at higher pressures after the phase transition. Correspondingly, the carrier lifetime first increases and then decreases with pressure. In both cases, the gap and the lifetime are anti-correlated. It is easier to study two different phases in experiment than calculation because the measurement time is sufficient to induce the structural change associated with the phase transition. The simulation timescale is very short, and one needs to perform separate calculations for each structure. The calculations combining real-time time domain DFT and NA-MD are much more computationally demanding than the common ab initio electronic structure calculations. The current work aimed to provide an atomistic rationalization of the unusual phenomenon observed in the experiments, rather than to repeat the experiments computationally. By considering one of the two phases, we were able to uncover the physical mechanisms rationalizing the unusual correlation. We chose the cubic structure to perform the calculations because it allows for a more straightforward analysis. The physical principles established in the current study should apply not only to the cubic $MAPbI_3$ but also to its other phases (tetragonal, orthorhombic) and to other perovskites.

Lattice mismatch between perovskites films and substrates can induce significant strain within the perovskites.[87] Perovskites are significantly softer and more responsive to strain than many other inorganic materials. For instance, perovskite bulk modulus an order of magnitude smaller than that of silicon.[88] Substrate-induced strain is both a practical reality that needs to be taken into account and a means to influence perovskite properties analogous to external pressure.

Pressure may not be the most optimal way to tune perovskite properties. Doping can achieve similar effects. In addition to halide doping, which influences carrier properties both structurally and electronically, one can also consider purely structural doping by replacing MA with different size cations, such as FA and GA. Both types of doping have been investigated in our previous works.[47,89] Pressure shrinks the lattice and changes the structural parameters, influencing the Pb-s and I-p anti-coupling and electron−vibrational interactions. Doping can also influence these structural parameters and thereby change the electronic properties near the band gap. Doping with larger A-site cations expands rather than contracts the lattice, and therefore, it is complimentary to external pressure. Smaller A-site cations have little influence on the Pb−I lattice. Doping with smaller halides acts to deform and shrink the lattice, similarly to pressure. In addition, smaller halogens are more electronegative than iodine and do not contribute to the VBM. Thus, they introduce disorder to the hole wavefunctions because holes can no longer occupy some of the X sites.

Our previous study[47] showed that doping with lighter halides reduces electron−hole overlap, speeds up the decoherence process by introducing higher frequency vibrations, and slows down charge recombination. Pressure induces similar effects: enhanced lattice disorder and fluctuations, charge localization, decreased electron−hole overlap, faster decoherence, and slower recombination. Doping with larger A-site cations has the opposite effect compared to pressure.[89] The lattice expands and becomes stiffer, and its fluctuations decrease. The electronic properties and the decoherence time change little, however, the NAC is reduced significantly. Thus, doping with either smaller or large ions allows stretching and compression that are similar to the pressure variation.

In summary, we have investigated the nonradiative charge recombination dynamics in the $MAPbI_3$ perovskite under different pressures using the state-of-the-art combination of ab initio time-domain DFT and NA-MD. The simulations indicate that pressure and strain provide effective means to control charge carrier relaxation. The simulations demonstrate that increasing pressure delays nonradiative charge recombination in $MAPbI_3$, in agreement with the experiments. Higher pressures destabilize the inorganic Pb−I lattice and increase thermal fluctuations of the Pb and I atoms, which support the VBM and CBM charge densities. At the same time, fluctuations of the MA cations are reduced. The enhanced thermal disorder localizes electron and hole charge densities, decreasing their overlap. Lattice contraction caused by the increased pressure shortens Pb−I bonds, distorts the $[PbI_6]^{4-}$ octahedra, and decreases the Pb−I−Pb bond angle. The lattice contraction brings the Pb and I atoms closer to each other, increases the antibonding coupling between the Pb-s and I-p orbitals, raises the VBM energy, and reduces the band gap. The enhanced fluctuations of the Pb and I atoms and the stronger charge localization shorten the quantum coherence time. Or equivalently, the destabilized Pb−I lattice responds more easily to the photoexcitation, leading to a smaller Franck−Condon factor for the excited-to-ground state transition. As a result, the nonradiative charge recombination slows down. The decreased band gap and increased carrier lifetime under compression form a favorable combination for improving efficiencies of solar energy devices. The study provides an atomistic rationalization of the experimental observations of the pressure-induced energy gap narrowing and carrier lifetime extension in $MAPbI_3$, generating important fundamental insights into the unusual properties of metal halide perovskites, needed for further optimization of these materials for optoelectronic applications.

■ ASSOCIATED CONTENT

Supporting Information

The Supporting Information is available free of charge at https://pubs.acs.org/doi/10.1021/acs.chemmater.0c01287.

Band structures, projected densities of states, influence of SOC on band gap curvature, time-dependent NAC, and average absolute atom velocities of $MAPbI_3$ under different pressures (PDF)

■ AUTHOR INFORMATION

Corresponding Authors

Wei Li − *School of Chemistry and Materials Science, Hunan Agricultural University, Changsha 410128, People's Republic of*

https://dx.doi.org/10.1021/acs.chemmater.0c01287
Chem. Mater. 2020, 32, 4707−4715

China; orcid.org/0000-0002-9999-5081; Email: weili@hunau.edu.cn

Oleg V. Prezhdo − *Department of Chemistry, University of Southern California, Los Angeles, California 90089, United States;* orcid.org/0000-0002-5140-7500; Email: prezhdo@usc.edu

Authors

Zhi Chen − *School of Chemistry and Materials Science, Hunan Agricultural University, Changsha 410128, People's Republic of China*

Jianfeng Tang − *School of Chemistry and Materials Science, Hunan Agricultural University, Changsha 410128, People's Republic of China*

Complete contact information is available at: https://pubs.acs.org/10.1021/acs.chemmater.0c01287

Notes

The authors declare no competing financial interest.

■ ACKNOWLEDGMENTS

W.L. acknowledges funding from Hunan Agricultural University (grant nos. 540741800499 and 18QN02), National Natural Science Foundation of China (grant no. 21903023), Natural Science Foundation of Hunan Province (grant no. 2020JJ1184). J.T. acknowledges Double first-class construction project of Hunan Agricultural University (no. SYL2019063) and Changsha Municipal Science and Technology Program (grant no. kq1801022). O.V.P. acknowledges funding from the U.S. National Science Foundation (grant no. CHE-1900510).

■ REFERENCES

(1) Xing, G.; Mathews, N.; Sun, S.; Lim, S. S.; Lam, Y. M.; Gratzel, M.; Mhaisalkar, S.; Sum, T. C. Long-Range Balanced Electron- and Hole-Transport Lengths in Organic-Inorganic $CH_3NH_3PbI_3$. *Science* **2013**, *342*, 344−347.

(2) Luo, D.; Su, R.; Zhang, W.; Gong, Q.; Zhu, R. Minimizing Non-Radiative Recombination Losses in Perovskite Solar Cells. *Nat. Rev. Mater.* **2020**, *5*, 44−60.

(3) Yang, J.; Wang, Y.; Wu, T.; Li, S. Correlating the Composition-Dependent Structural and Electronic Dynamics of Inorganic Mixed Halide Perovskites. *Chem. Mater.* **2020**, *32*, 2470−2481.

(4) Yin, J.; Yang, H.; Song, K.; El-Zohry, A. M.; Han, Y.; Bakr, O. M.; Brédas, J.-L.; Mohammed, O. F. Point Defects and Green Emission in Zero-Dimensional Perovskites. *J. Phys. Chem. Lett.* **2018**, *9*, 5490−5495.

(5) Mir, W. J.; Mahor, Y.; Lohar, A.; Jagadeeswararao, M.; Das, S.; Mahamuni, S.; Nag, A. Postsynthesis Doping of Mn and Yb into $CsPbX_3$ (X = Cl, Br, or I) Perovskite Nanocrystals for Down-conversion Emission. *Chem. Mater.* **2018**, *30*, 8170−8178.

(6) Ball, J. M.; Petrozza, A. Defects in Perovskite-Halides and Their Effects in Solar Cells. *Nat. Energy* **2016**, *1*, 2016149.

(7) Boziki, A.; Kubicki, D. J.; Mishra, A.; Meloni, S.; Emsley, L.; Grätzel, M.; Rothlisberger, U. Atomistic Origins of the Limited Phase Stability of Cs^+-Rich $FA_xCs_{(1-x)}PbI_3$ Mixtures. *Chem. Mater.* **2020**, *32*, 2605−2614.

(8) Zhang, X.; Shen, J. X.; Van de Walle, C. G. First-Principles Simulation of Carrier Recombination Mechanisms in Halide Perovskites. *Adv. Energy Mater.* **2020**, *10*, 1902830.

(9) Best Research Cell Efficiency; National Renewable Energy Laboratory, https://www.nrel.gov/pv/assets/pdfs/best-research-cell-efficiencies.20190802.pdf (accessed Aug 2, 2019).

(10) Shockley, W.; Queisser, H. J. Detailed Balance Limit of Efficiency of p−n Junction Solar Cells. *J. Appl. Phys.* **1961**, *32*, 510−519.

(11) He, J.; Vasenko, A. S.; Long, R.; Prezhdo, O. V. Halide Composition Controls Electron−Hole Recombination in Cesium−Lead Halide Perovskite Quantum Dots: A Time Domain Ab Initio Study. *J. Phys. Chem. Lett.* **2018**, *9*, 1872−1879.

(12) Xu, W.; Liu, L.; Yang, L.; Shen, P.; Sun, B.; McLeod, J. A. Dissociation of Methylammonium Cations in Hybrid Organic−Inorganic Perovskite Solar Cells. *Nano Lett.* **2016**, *16*, 4720−4725.

(13) Han, T. H.; Tan, S.; Xue, J.; Meng, L.; Lee, J. W.; Yang, Y. Interface and Defect Engineering for Metal Halide Perovskite Optoelectronic Devices. *Adv. Mater.* **2019**, *31*, 1803515.

(14) Fu, X.; Dong, N.; Lian, G.; Lv, S.; Zhao, T.; Wang, Q.; Cui, D.; Wong, C.-P. High-Quality $CH_3NH_3PbI_3$ Films Obtained via a Pressure-Assisted Space-Confined Solvent-Engineering Strategy for Ultrasensitive Photodetectors. *Nano Lett.* **2018**, *18*, 1213−1220.

(15) Im, J.; Stoumpos, C. C.; Jin, H.; Freeman, A. J.; Kanatzidis, M. G. Antagonism between Spin−Orbit Coupling and Steric Effects Causes Anomalous Band Gap Evolution in the Perovskite Photovoltaic Materials $CH_3NH_3Sn_{1-x}Pb_xI_3$. *J. Phys. Chem. Lett.* **2015**, *6*, 3503−3509.

(16) Jaffe, A.; Lin, Y.; Karunadasa, H. I. Halide Perovskites under Pressure: Accessing New Properties through Lattice Compression. *ACS Energy Lett.* **2017**, *2*, 1549−1555.

(17) Szafrański, M.; Katrusiak, A. Photovoltaic Hybrid Perovskites under Pressure. *J. Phys. Chem. Lett.* **2017**, *8*, 2496−2506.

(18) Liu, X. C.; Han, J. H.; Zhao, H. F.; Yan, H. C.; Shi, Y.; Jin, M. X.; Liu, C. L.; Ding, D. J. Pressure Dependence of Excited-State Charge-Carrier Dynamics in Organolead Tribromide Perovskites. *Appl. Phys. Lett.* **2018**, *112*, 191903.

(19) Beimborn, J. C.; Hall, L. M. G.; Tongying, P.; Dukovic, G.; Weber, J. M. Pressure Response of Photoluminescence in Cesium Lead Iodide Perovskite Nanocrystals. *J. Phys. Chem. C* **2018**, *122*, 11024−11030.

(20) Jiang, S.; Fang, Y.; Li, R.; Xiao, H.; Crowley, J.; Wang, C.; White, T. J.; Goddard, W. A.; Wang, Z.; Baikie, T.; Fang, J. Pressure-Dependent Polymorphism and Band-Gap Tuning of Methylammonium Lead Iodide Perovskite. *Angew. Chem., Int. Ed.* **2016**, *55*, 6540−6544.

(21) Liu, G.; Kong, L.; Gong, J.; Yang, W.; Mao, H.-k.; Hu, Q.; Liu, Z.; Schaller, R. D.; Zhang, D.; Xu, T. Pressure-Induced Band gap Optimization in Lead-Based Perovskites with Prolonged Carrier Lifetime and Ambient Retainability. *Adv. Funct. Mater.* **2017**, *27*, 1604208.

(22) Akimov, A. V.; Prezhdo, O. V. The PYXAID Program for Non-Adiabatic Molecular Dynamics in Condensed Matter Systems. *J. Chem. Theory Comput.* **2013**, *9*, 4959−4972.

(23) Craig, C. F.; Duncan, W. R.; Prezhdo, O. V. Trajectory Surface Hopping in the Time-Dependent Kohn-Sham Approach for Electron-Nuclear Dynamics. *Phys. Rev. Lett.* **2005**, *95*, 163001.

(24) Kong, L.; Liu, G.; Gong, J.; Hu, Q.; Schaller, R. D.; Dera, P.; Zhang, D.; Liu, Z.; Yang, W.; Zhu, K.; Tang, Y.; Wang, C.; Wei, S.-H.; Xu, T.; Mao, H.-k. Simultaneous Band-Gap Narrowing and Carrier-Lifetime Prolongation of Organic−Inorganic Trihalide Perovskites. *Proc. Natl. Acad. Sci. U.S.A.* **2016**, *113*, 8910−8915.

(25) Jiang, S.; Luan, Y.; Jang, J. I.; Baikie, T.; Huang, X.; Li, R.; Saouma, F. O.; Wang, Z.; White, T. J.; Fang, J. Phase Transitions of Formamidinium Lead Iodide Perovskite under Pressure. *J. Am. Chem. Soc.* **2018**, *140*, 13952−13957.

(26) Englman, R.; Jortner, J. The Energy Gap Law for Radiationless Transitions in Large Molecules. *Mol. Phys.* **1970**, *18*, 145−164.

(27) Zhang, L.; Zeng, Q.; Wang, K. Pressure-Induced Structural and Optical Properties of Inorganic Halide Perovskite $CsPbBr_3$. *J. Phys. Chem. Lett.* **2017**, *8*, 3752−3758.

(28) Xiao, G.; Cao, Y.; Qi, G.; Wang, L.; Liu, C.; Ma, Z.; Yang, X.; Sui, Y.; Zheng, W.; Zou, B. Pressure Effects on Structure and Optical Properties in Cesium Lead Bromide Perovskite Nanocrystals. *J. Am. Chem. Soc.* **2017**, *139*, 10087−10094.

(29) Jaeger, H. M.; Fischer, S.; Prezhdo, O. V. Decoherence-Induced Surface Hopping. *J. Chem. Phys.* **2012**, *137*, 22A545.

(30) Akimov, A. V.; Prezhdo, O. V. Advanced Capabilities of the PYXAID Program: Integration Schemes, Decoherence Effects, Multiexcitonic States, and Field-Matter Interaction. *J. Chem. Theory Comput.* **2014**, *10*, 789−804.
(31) Mukamel, S. *Principles of Nonlinear Optical Spectroscopy*; Oxford Series in Optical and Imaging Sciences; Oxford University Press: Oxford, New York, 1999.
(32) Zhou, X.; Tokina, M. V.; Tomko, J. A.; Braun, J. L.; Hopkins, P. E.; Prezhdo, O. V. Thin Ti Adhesion Layer Breaks Bottleneck to Hot Hole Relaxation in Au Films. *J. Chem. Phys.* **2019**, *150*, 184701.
(33) Zhang, J.; Guan, M.; Lischner, J.; Meng, S.; Prezhdo, O. V. Coexistence of Different Charge-Transfer Mechanisms in the Hot-Carrier Dynamics of Hybrid Plasmonic Nanomaterials. *Nano Lett.* **2019**, *19*, 3187−3193.
(34) Syzgantseva, M. A.; Stepanov, N. F.; Syzgantseva, O. A. Carrier Lifetimes and Recombination Pathways in Metal−Organic Frameworks. *J. Phys. Chem. Lett.* **2019**, *10*, 5041−5046.
(35) Nam, Y.; Li, L.; Lee, J. Y.; Prezhdo, O. V. Strong Influence of Oxygen Vacancy Location on Charge Carrier Losses in Reduced TiO_2 Nanoparticles. *J. Phys. Chem. Lett.* **2019**, *10*, 2676−2683.
(36) Li, W.; Long, R.; Hou, Z.; Tang, J.; Prezhdo, O. V. Influence of Encapsulated Water on Luminescence Energy, Line Width, and Lifetime of Carbon Nanotubes: Time Domain Ab Initio Analysis. *J. Phys. Chem. Lett.* **2018**, *9*, 4006−4013.
(37) Li, L.; Long, R.; Prezhdo, O. V. Charge Separation and Recombination in Two-Dimensional MoS_2/WS_2: Time-Domain Ab Initio Modeling. *Chem. Mater.* **2017**, *29*, 2466−2473.
(38) Long, R.; Casanova, D.; Fang, W.-H.; Prezhdo, O. V. Donor−Acceptor Interaction Determines the Mechanism of Photoinduced Electron Injection from Graphene Quantum Dots into TiO_2: π-Stacking Supersedes Covalent Bonding. *J. Am. Chem. Soc.* **2017**, *139*, 2619−2629.
(39) Wang, L.; Long, R.; Prezhdo, O. V. Time-Domain Ab Initio Modeling of Photoinduced Dynamics at Nanoscale Interfaces. *Annu. Rev. Phys. Chem.* **2015**, *66*, 549−579.
(40) Zhang, L.; Vasenko, A. S.; Zhao, J.; Prezhdo, O. V. Mono-Elemental Properties of 2D Black Phosphorus Ensure Extended Charge Carrier Lifetimes under Oxidation: Time-Domain Ab Initio Analysis. *J. Phys. Chem. Lett.* **2019**, *10*, 1083−1091.
(41) Zhang, Z.; Long, R. Doping-Induced Rapid Decoherence Suppresses Charge Recombination in Mono/Divalent Cation Mixed Perovskites from Nonadiabatic Molecular Dynamics Simulation. *J. Phys. Chem. Lett.* **2019**, *10*, 3433−3439.
(42) Li, W.; Zhang, X.; Lu, G. Unraveling Photoexcitation Dynamics at "Dots-in-a-Perovskite" Heterojunctions from First-Principles. *J. Mater. Chem. A* **2019**, *7*, 18012−18019.
(43) Wang, Y.; He, J.; Yang, Y.; Zhang, Z.; Long, R. Chlorine Passivation of Grain Boundary Suppresses Electron-Hole Recombination in $CsPbBr_3$ Perovskite by Nonadiabatic Molecular Dynamics Simulation. *ACS Appl. Energy Mater.* **2019**, *2*, 3419−3426.
(44) Li, W.; Liu, J.; Bai, F.-Q.; Zhang, H.-X.; Prezhdo, O. V. Hole Trapping by Iodine Interstitial Defects Decreases Free Carrier Losses in Perovskite Solar Cells: A Time-Domain *Ab Initio* Study. *ACS Energy Lett.* **2017**, *2*, 1270−1278.
(45) Long, R.; Fang, W.; Prezhdo, O. V. Moderate Humidity Delays Electron−Hole Recombination in Hybrid Organic−Inorganic Perovskites: Time-Domain Ab Initio Simulations Rationalize Experiments. *J. Phys. Chem. Lett.* **2016**, *7*, 3215−3222.
(46) Long, R.; Prezhdo, O. V. Dopants Control Electron−Hole Recombination at Perovskite−TiO_2 Interfaces: Ab Initio Time-Domain Study. *ACS Nano* **2015**, *9*, 11143−11155.
(47) Liu, J.; Prezhdo, O. V. Chlorine Doping Reduces Electron−Hole Recombination in Lead Iodide Perovskites: Time-Domain Ab Initio Analysis. *J. Phys. Chem. Lett.* **2015**, *6*, 4463−4469.
(48) Li, W.; Vasenko, A. S.; Tang, J.; Prezhdo, O. V. Anharmonicity Extends Carrier Lifetimes in Lead Halide Perovskites at Elevated Temperatures. *J. Phys. Chem. Lett.* **2019**, *10*, 6219−6226.
(49) Zhang, Z.; Fang, W.-H.; Long, R.; Prezhdo, O. V. Exciton Dissociation and Suppressed Charge Recombination at 2D Perovskite Edges: Key Roles of Unsaturated Halide Bonds and Thermal Disorder. *J. Am. Chem. Soc.* **2019**, *141*, 15557−15566.
(50) He, J.; Fang, W.-H.; Long, R.; Prezhdo, O. V. Superoxide/Peroxide Chemistry Extends Charge Carriers Lifetime but Undermines Chemical Stability of $CH_3NH_3PbI_3$ Exposed to Oxygen: Time-Domain Ab Initio Analysis. *J. Am. Chem. Soc.* **2019**, *141*, 5798−5807.
(51) Yin, J.; Maity, P.; Naphade, R.; Cheng, B.; He, J.-H.; Bakr, O. M.; Brédas, J.-L.; Mohammed, O. F. Tuning Hot Carrier Cooling Dynamics by Dielectric Confinement in Two-Dimensional Hybrid Perovskite Crystals. *ACS Nano* **2019**, *13*, 12621−12629.
(52) Zhang, S.-F.; Chen, X.-K.; Ren, A.-M.; Li, H.; Bredas, J.-L. Impact of Organic Spacers on the Carrier Dynamics in 2D Hybrid Lead-Halide Perovskites. *ACS Energy Lett.* **2019**, *4*, 17−25.
(53) Baikie, T.; Fang, Y.; Kadro, J. M.; Schreyer, M.; Wei, F.; Mhaisalkar, S. G.; Graetzel, M.; White, T. J. Synthesis and Crystal Chemistry of the Hybrid Perovskite $(CH_3NH_3)PbI_3$ for Solid-State Sensitised Solar Cell Applications. *J. Mater. Chem. A* **2013**, *1*, 5628−5641.
(54) Quarti, C.; De Angelis, F.; Beljonne, D. Influence of Surface Termination on the Energy Level Alignment at the $CH_3NH_3PbI_3$ Perovskite/C60 Interface. *Chem. Mater.* **2017**, *29*, 958−968.
(55) Taylor, V. C. A.; Tiwari, D.; Duchi, M.; Donaldson, P. M.; Clark, I. P.; Fermin, D. J.; Oliver, T. A. A. Investigating the Role of the Organic Cation in Formamidinium Lead Iodide Perovskite Using Ultrafast Spectroscopy. *J. Phys. Chem. Lett.* **2018**, *9*, 895−901.
(56) Tong, C.-J.; Geng, W.; Prezhdo, O. V.; Liu, L.-M. Role of Methylammonium Orientation in Ion Diffusion and Current−Voltage Hysteresis in the $CH_3NH_3PbI_3$ Perovskite. *ACS Energy Lett.* **2017**, *2*, 1997−2004.
(57) Giorgi, G.; Fujisawa, J.-I.; Segawa, H.; Yamashita, K. Small Photocarrier Effective Masses Featuring Ambipolar Transport in Methylammonium Lead Iodide Perovskite: A Density Functional Analysis. *J. Phys. Chem. Lett.* **2013**, *4*, 4213−4216.
(58) Kresse, G.; Hafner, J. *Ab Initio* Molecular Dynamics for Liquid Metals. *Phys. Rev. B: Condens. Matter Mater. Phys.* **1993**, *47*, 558−561.
(59) Kresse, G.; Hafner, J. *Ab Initio* Molecular-Dynamics Simulation of the Liquid-Metal−Amorphous-Semiconductor Transition in Germanium. *Phys. Rev. B: Condens. Matter Mater. Phys.* **1994**, *49*, 14251−14269.
(60) Li, W.; Zhou, L.; Prezhdo, O. V.; Akimov, A. V. Spin-Orbit Interactions Greatly Accelerate Nonradiative Dynamics in Lead Halide Perovskites. *ACS Energy Lett.* **2018**, *3*, 2159−2166.
(61) Even, J.; Pedesseau, L.; Jancu, J.-M.; Katan, C. Importance of Spin−Orbit Coupling in Hybrid Organic/Inorganic Perovskites for Photovoltaic Applications. *J. Phys. Chem. Lett.* **2013**, *4*, 2999−3005.
(62) Quarti, C.; Marchal, N.; Beljonne, D. Tuning the Optoelectronic Properties of Two-Dimensional Hybrid Perovskite Semiconductors with Alkyl Chain Spacers. *J. Phys. Chem. Lett.* **2018**, *9*, 3416−3424.
(63) Umari, P.; Mosconi, E.; De Angelis, F. Relativistic GW Calculations on $CH_3NH_3PbI_3$ and $CH_3NH_3SnI_3$ Perovskites for Solar Cell Applications. *Sci. Rep.* **2014**, *4*, 4467.
(64) Li, W.; Sun, Y.-Y.; Li, L.; Zhou, Z.; Tang, J.; Prezhdo, O. V. Control of Charge Recombination in Perovskites by Oxidation State of Halide Vacancy. *J. Am. Chem. Soc.* **2018**, *140*, 15753−15763.
(65) Wang, Y.; Long, R. Unravelling the Effects of Pressure-Induced Suppressed Electron−Hole Recombination in $CsPbBr_3$ Perovskite: Time-Domain Ab Initio Analysis. *J. Phys. Chem. Lett.* **2019**, *10*, 4354−4361.
(66) Li, W.; Long, R.; Tang, J.; Prezhdo, O. V. Influence of Defects on Excited-State Dynamics in Lead Halide Perovskites: Time-Domain ab Initio Studies. *J. Phys. Chem. Lett.* **2019**, *10*, 3788−3804.
(67) Li, W.; Tang, J.; Casanova, D.; Prezhdo, O. V. Time-Domain Ab Initio Analysis Rationalizes the Unusual Temperature Dependence of Charge Carrier Relaxation in Lead Halide Perovskite. *ACS Energy Lett.* **2018**, *3*, 2713−2720.
(68) Wang, Y.; Fang, W.-H.; Long, R.; Prezhdo, O. V. Symmetry Breaking at $MAPbI_3$ Perovskite Grain Boundaries Suppresses Charge

https://dx.doi.org/10.1021/acs.chemmater.0c01287
Chem. Mater. 2020, 32, 4707−4715

Recombination: Time-Domain Ab Initio Analysis. *J. Phys. Chem. Lett.* **2019**, *10*, 1617−1623.
(69) Yin, W.-J.; Shi, T.; Yan, Y. Unusual Defect Physics in $CH_3NH_3PbI_3$ Perovskite Solar Cell Absorber. *Appl. Phys. Lett.* **2014**, *104*, 063903.
(70) Ghosh, D.; Acharya, D.; Zhou, L.; Nie, W.; Prezhdo, O. V.; Tretiak, S.; Neukirch, A. J. Lattice Expansion in Hybrid Perovskites: Effect on Optoelectronic Properties and Charge Carrier Dynamics. *J. Phys. Chem. Lett.* **2019**, *10*, 5000−5007.
(71) Ghosh, D.; Smith, A. R.; Walker, A. B.; Islam, M. S. Mixed A-Cation Perovskites for Solar Cells: Atomic-Scale Insights Into Structural Distortion, Hydrogen Bonding, and Electronic Properties. *Chem. Mater.* **2018**, *30*, 5194−5204.
(72) Akimov, A. V.; Prezhdo, O. V. Persistent Electronic Coherence Despite Rapid Loss of Electron−Nuclear Correlation. *J. Phys. Chem. Lett.* **2013**, *4*, 3857−3864.
(73) Kilina, S. V.; Neukirch, A. J.; Habenicht, B. F.; Kilin, D. S.; Prezhdo, O. V. Quantum Zeno Effect Rationalizes the Phonon Bottleneck in Semiconductor Quantum Dots. *Phys. Rev. Lett.* **2013**, *110*, 180404.
(74) Ghosh, D.; Aziz, A.; Dawson, J. A.; Walker, A. B.; Islam, M. S. Putting the Squeeze on Lead Iodide Perovskites: Pressure-Induced Effects To Tune Their Structural and Optoelectronic Behavior. *Chem. Mater.* **2019**, *31*, 4063−4071.
(75) Francisco-López, A.; Charles, B.; Weber, O. J.; Alonso, M. I.; Garriga, M.; Campoy-Quiles, M.; Weller, M. T.; Goñi, A. R. Pressure-Induced Locking of Methylammonium Cations versus Amorphization in Hybrid Lead Iodide Perovskites. *J. Phys. Chem. C* **2018**, *122*, 22073−22082.
(76) Capitani, F.; Marini, C.; Caramazza, S.; Dore, P.; Pisanu, A.; Malavasi, L.; Nataf, L.; Baudelet, F.; Brubach, J.-B.; Roy, P.; Postorino, P. Locking of Methylammonium by Pressure-Enhanced H-Bonding in $(CH_3NH_3)PbBr_3$ Hybrid Perovskite. *J. Phys. Chem. C* **2017**, *121*, 28125−28131.
(77) Prezhdo, O. V.; Rossky, P. J. Evaluation of Quantum Transition Rates from Quantum-Classical Molecular Dynamics Simulations. *J. Chem. Phys.* **1997**, *107*, 5863−5878.
(78) Habenicht, B. F.; Kamisaka, H.; Yamashita, K.; Prezhdo, O. V. Ab Initio Study of Vibrational Dephasing of Electronic Excitations in Semiconducting Carbon Nanotubes. *Nano Lett.* **2007**, *7*, 3260−3265.
(79) Smith, B.; Akimov, A. V. A Comparative Analysis of Surface Hopping Acceptance and Decoherence Algorithms within the Neglect of Back-Reaction Approximation. *J. Chem. Phys.* **2019**, *151*, 124107.
(80) DiVincenzo, D. P.; Loss, D. Quantum Computers and Quantum Coherence. *J. Magn. Magn. Mater.* **1999**, *200*, 202−218.
(81) Prezhdo, O. V. Quantum Anti-Zeno Acceleration of a Chemical Reaction. *Phys. Rev. Lett.* **2000**, *85*, 4413−4417.
(82) Quarti, C.; Grancini, G.; Mosconi, E.; Bruno, P.; Ball, J. M.; Lee, M. M.; Snaith, H. J.; Petrozza, A.; De Angelis, F. The Raman Spectrum of the $CH_3NH_3PbI_3$ Hybrid Perovskite: Interplay of Theory and Experiment. *J. Phys. Chem. Lett.* **2014**, *5*, 279−284.
(83) Hedley, G. J.; Quarti, C.; Harwell, J.; Prezhdo, O. V.; Beljonne, D.; Samuel, I. D. W. Hot-Hole Cooling Controls the Initial Ultrafast Relaxation in Methylammonium Lead Iodide Perovskite. *Sci. Rep.* **2018**, *8*, 8115.
(84) Madjet, M. E.-A.; Akimov, A. V.; El-Mellouhi, F.; Berdiyorov, G. R.; Ashhab, S.; Tabet, N.; Kais, S. Enhancing the Carrier Thermalization Time in Organometallic Perovskites by Halide Mixing. *Phys. Chem. Chem. Phys.* **2016**, *18*, 5219−5231.
(85) Miyata, K.; Atallah, T. L.; Zhu, X.-Y. Lead Halide Perovskites: Crystal-Liquid Duality, Phonon Glass Electron Crystals, and Large Polaron Formation. *Sci. Adv.* **2017**, *3*, No. e1701469.
(86) Long, R.; Liu, J.; Prezhdo, O. V. Unravelling the Effects of Grain Boundary and Chemical Doping on Electron−Hole Recombination in $CH_3NH_3PbI_3$ Perovskite by Time-Domain Atomistic Simulation. *J. Am. Chem. Soc.* **2016**, *138*, 3884−3890.
(87) Chen, Y.; Lei, Y.; Li, Y.; Yu, Y.; Cai, J.; Chiu, M.-H.; Rao, R.; Gu, Y.; Wang, C.; Choi, W.; Hu, H.; Wang, C.; Li, Y.; Song, J.; Zhang, J.; Qi, B.; Lin, M.; Zhang, Z.; Islam, A. E.; Maruyama, B.; Dayeh, S.; Li, L.-J.; Yang, K.; Lo, Y.-H.; Xu, S. Strain Engineering and Epitaxial Stabilization of Halide Perovskites. *Nature* **2020**, *577*, 209−215.
(88) Stavrakas, C.; Zelewski, S. J.; Frohna, K.; Booker, E. P.; Galkowski, K.; Ji, K.; Ruggeri, E.; Mackowski, S.; Kudrawiec, R.; Plochocka, P.; Stranks, S. D. Influence of Grain Size on Phase Transitions in Halide Perovskite Films. *Adv. Energy Mater.* **2019**, *9*, 1901883.
(89) He, J.; Fang, W.-H.; Long, R.; Prezhdo, O. V. Increased Lattice Stiffness Suppresses Nonradiative Charge Recombination in $MAPbI_3$ Doped with Larger Cations: Time-Domain Ab Initio Analysis. *ACS Energy Lett.* **2018**, *3*, 2070−2076.

https://dx.doi.org/10.1021/acs.chemmater.0c01287
Chem. Mater. 2020, 32, 4707−4715